CrossMark

Soft-lubrication interactions between a rigid sphere and an elastic wall

Vincent Bertin[1,2], **Yacine Amarouchene**[1], **Elie Raphaël**[2] and **Thomas Salez**[1,3],†

[1]Univ. Bordeaux, CNRS, LOMA, UMR 5798, 33405 Talence, France

[2]UMR CNRS Gulliver 7083, ESPCI Paris, PSL Research University, 75005 Paris, France

[3]Global Station for Soft Matter, Global Institution for Collaborative Research and Education, Hokkaido University, Sapporo, Hokkaido 060-0808, Japan

The motion of an object within a viscous fluid and in the vicinity of a soft surface induces a hydrodynamic stress field that deforms the latter, thus modifying the boundary conditions of the flow. This results in elastohydrodynamic interactions experienced by the particle. Here, we derive a soft-lubrication model, in order to compute all the forces and torque applied on a rigid sphere that is free to translate and rotate near an elastic wall. We focus on the limit of small deformations of the surface with respect to the fluid-gap thickness, and perform a perturbation analysis in dimensionless compliance. The response is computed in the framework of linear elasticity, for planar elastic substrates in the limiting cases of thick and thin layers. The EHD forces are also obtained analytically using the Lorentz reciprocal theorem.

1. Introduction

The fluid-structure interaction between flows and boundaries is a central situation in continuum mechanics, encountered at many length and velocity scales. A classical example is lubrication, where the addition of a liquid film – a lubricant – between two contacting objects allows for a drastic reduction of the friction between them. Such a process occurs in a large variety of contexts with hard materials, such as roller bearings, pistons and gears in industry (Dowson & Higginson 2014), or faults (Brodsky & Kanamori 2001) and landslides (Campbell 1989) in geological settings. At large velocity, or moderate loading, the liquid film is continuous with no direct contact between the solids. When the

† Email address for correspondence: thomas.salez@u-bordeaux.fr

solids are deformable, the friction force can be described using elastohydrodynamic (EHD) models within the soft-lubrication approximation (Dowson & Higginson 2014).

The previous EHD coupling is also widely encountered in soft condensed matter, but at very different pressure and velocity scales (Karan, Chakraborty & Chakraborty 2018). Examples encompass the remarkable frictional properties of eyelids (Jones *et al.* 2008) and cartilaginous joints (Mow, Holmes & Lai 1984; Jahn, Seror & Klein 2016), as well as biomimetic gels (Gong 2006) and rubbers (Sekimoto & Leibler 1993; Moyle *et al.* 2020; Wu *et al.* 2020; Hui *et al.* 2021). Of interest as well are the collisions and rebounds of spheres in viscous environments (Davis, Serayssol & Hinch 1986; Gondret, Lance & Petit 2002; Tan, Wang & Frechette 2019), the rheological properties of soft suspensions and pastes (Sekimoto & Leibler 1993; Meeker, Bonnecaze & Cloitre 2004), and the self-similar properties of the contact (Snoeijer, Eggers & Venner 2013).

In the last decade, EHD interactions have been of great interest in the materials science community with the emergence of contactless rheological methods to measure the mechanical properties of confined liquids and soft surfaces (Chan, Klaseboer & Manica 2009; Vakarelski *et al.* 2010; Leroy & Charlaix 2011; Leroy *et al.* 2012; Villey *et al.* 2013; Wang, Dhong & Frechette 2015; Guan *et al.* 2017; Wang *et al.* 2017*a*; Wang, Tan & Frechette 2017*b*; Wang *et al.* 2018; Lainé *et al.* 2019; Bertin *et al.* 2021). Typically, in such experimental systems, a spherical colloidal probe is immersed in a fluid and driven to oscillate, with a nanometric amplitude, near a surface of interest. The force exerted on the probe is measured by an atomic force microscope, a surface force apparatus or a tuning-fork microscope, and depends on the properties of both the fluid and the solid boundary.

Generally, an object that moves in a confined fluid environment experiences an enhanced drag force with respect to the bulk Stokes law, as a result of the boundary-induced flow modification (Happel & Brenner 2012). Furthermore, near a soft wall, the hydrodynamic interactions are modified by the deformation of the boundary that they generate, yielding a nonlinear coupling. Perturbation methods, assuming a small deformation of the interface, have been employed in order to calculate the soft-lubrication interactions exerted on a free infinite cylinder immersed in a viscous fluid and near a thin compressible elastic material (Salez & Mahadevan 2015). In particular, interesting inertial-like features have been predicted despite the low-*Re*-number aspect of the flow.

Perhaps the most emblematic example of soft-lubrication interaction is the non-inertial lift force predicted for a particle sliding near a soft boundary (Sekimoto & Leibler 1993; Beaucourt, Biben & Misbah 2004; Skotheim & Mahadevan 2004, 2005; Urzay, Llewellyn Smith & Glover 2007; Urzay 2010). It might have important implications for advected biological entities, such as red blood cells (Grandchamp *et al.* 2013) and vesicles (Abkarian, Lartigue & Viallat 2002). Only recently, the associated dynamical repulsion from an immersed soft interface has been studied experimentally. A preliminary qualitative observation was reported in the context of smart lubricants and elastic polyelectrolytes (Bouchet *et al.* 2015). Then a study involving the sliding of an immersed macroscopic cylinder along an inclined plane pre-coated with a thin layer of gel, showed quantitatively an effective reduction of friction induced by the EHD lift force (Saintyves *et al.* 2016). Subsequently, the same effect was observed in the trajectories of micrometric spherical beads within a microfluidic channel coated with a biomimetic polymer layer (Davies *et al.* 2018), and through the sedimentation of a macroscopic sphere near a pre-tensed suspended elastic membrane (Rallabandi *et al.* 2018). Finally, direct measurements of the EHD lift force for two types of elastic materials have been performed at small scales, using surface

force apparatus and atomic force microscopy, respectively (Vialar *et al.* 2019; Zhang *et al.* 2020).

Despite the increasing number of EHD studies involving spherical probes, the soft-lubrication interactions of a free spherical object immersed in a viscous fluid and moving near an elastic substrate still have to be calculated. In the present article, we aim at filling this gap by deriving a soft-lubrication perturbation theory, in order to compute all the forces and torque for this problem, at first order in dimensionless compliance.

The article is organized as follows. First, we introduce the soft-lubrication framework for a sphere translating near a soft planar surface, in both normal and tangential directions. The substrate deformation is assumed to follow the constitutive response of a linear elastic semi-infinite material. Then we follow a perturbative approach, assuming the substrate deformation to be small with respect to the fluid-gap thickness, which allows us to find the normal and tangential forces as well as the torque experienced by the sphere, at first order in dimensionless compliance. Finally, we discuss the rotation of the sphere, before providing concluding remarks. Besides, in Appendices A–D, the EHD forces are computed analytically using the Lorentz reciprocal theorem, while the procedure introduced in the main text is reproduced for the compressible and incompressible responses of a thin material.

2. Model

The system is depicted in figure 1. We consider a sphere of radius a, immersed in a Newtonian fluid of dynamic shear viscosity η and density ρ. The sphere is moving with a tangential velocity $\boldsymbol{u}(t) = u(t)\, \boldsymbol{e}_x$ directed along the x-axis (by definition of the latter axis), where $\boldsymbol{e}_j$ denotes the unit vector along j. In this first part, we assume that the sphere does not rotate, i.e. the angular velocity reads $\boldsymbol{\Omega} = \boldsymbol{0}$. The sphere is placed at a time-dependent distance $d(t)$ (thus a $\dot{d}\boldsymbol{e}_z$ normal velocity of the sphere) of an isotropic and homogeneous linear elastic substrate of Lamé coefficients λ and μ, with a reference undeformed flat surface in the xy-plane at $z = 0$. We suppose that the sphere–wall distance is small with respect to the sphere radius, such that the lubrication approximation is valid. The fluid inertia is neglected here. Specifically, we assume $Re(d/a) \ll 1$, with the Reynolds number $Re = \rho u a / \eta$. Furthermore, we suppose that the typical time scale of variation of the sphere velocity is much larger than the diffusion time scale of vorticity that scales as $d^2/(\eta/\rho)$, such that the flow is described by the steady Stokes equations. This amounts to assuming that $|\dot{u}/u| \ll \eta/(\rho d^2)$ and $|\ddot{d}/\dot{d}| \ll \eta/(\rho d^2)$. We stress that slippage at solid surfaces modifies the lubrication pressure as well as the EHD interaction (Vinogradova & Feuillebois 2000), which is of importance for flows at the nanoscale (Bocquet & Charlaix 2010). Here, we ignore this effect and no-slip boundary conditions are assumed at both the sphere and wall surfaces. Finally, the system is equivalent to a sphere at rest near a wall translating with a $-(d(t)\, \boldsymbol{e}_z + \boldsymbol{u}(t))$ velocity. In such a framework, the fluid velocity field can be written as

$$\boldsymbol{v}(\boldsymbol{r}, z, t) = \frac{\nabla p(\boldsymbol{r}, t)}{2\eta}(z - h_0(\boldsymbol{r}, t))(z - \delta(\boldsymbol{r}, t)) - \boldsymbol{u}(t)\, \frac{h_0(\boldsymbol{r}, t) - z}{h_0(\boldsymbol{r}, t) - \delta(\boldsymbol{r}, t)}, \quad (2.1)$$

where $\boldsymbol{r} = (r, \theta)$ is the position in the tangential plane xy, ∇ is the two-dimensional gradient operator on xy, $\delta(\boldsymbol{r}, t)$ is the substrate deformation, and $z = h_0(\boldsymbol{r}, t)$ is the sphere surface. Near contact, the latter can be approximated by its parabolic expansion

$h_0(r, t) \simeq d(t) + r^2/(2a)$. Volume conservation further leads to the Reynolds equation

$$\partial_t h(r, t) = \nabla \cdot \left(\frac{h^3(r, t)}{12\eta} \nabla p(r, t) + \frac{h(r, t)}{2} u(t) \right), \tag{2.2}$$

where $h(r, t) = h_0(r, t) - \delta(r, t)$ is the fluid-gap thickness. In this first part, we assume that the constitutive elastic response is linear and instantaneous, and that the substrate is a semi-infinite medium, such that the deformation reads (Davis *et al.* 1986)

$$\delta(r, t) = -\frac{(\lambda + 2\mu)}{4\pi\mu(\lambda + \mu)} \int_{\mathbb{R}^2} \mathrm{d}^2x \, \frac{p(x, t)}{|r - x|}. \tag{2.3}$$

We non-dimensionalize the problem through

$$h(r, t) = d^* H(R, T), \quad r = \sqrt{2ad^*} R, \quad d(t) = d^* D(T), \quad \delta(r, t) = d^* \Delta(R, T), \tag{2.4a–d}$$

$$p(r, t) = \frac{\eta u^* \sqrt{2ad^*}}{d^{*2}} P(R, T), \quad u(t) = u^* U(T) \, e_x, \quad v = u^* V, \quad t = \frac{\sqrt{2ad^*}}{u^*} T, \tag{2.5a–d}$$

where d^* and u^* are characteristic fluid-gap distance and tangential velocity, respectively. The governing equations are then

$$12\partial_T H(R, T) = \nabla \cdot \left(H^3(R, T) \nabla P(R, T) + 6H(R, T) U(T) \right), \tag{2.6}$$

$$H(R, T) = D(T) + R^2 - \Delta(R, T) \tag{2.7}$$

and

$$\Delta(R, T) = -\kappa \int_{\mathbb{R}^2} \mathrm{d}^2X \, \frac{P(X, T)}{4\pi|R - X|}, \tag{2.8}$$

where we introduced the dimensionless compliance

$$\kappa = \frac{2\eta u^* a(\lambda + 2\mu)}{d^{*2}\mu(\lambda + \mu)}. \tag{2.9}$$

The latter is the only dimensionless parameter in the problem. When κ is small with respect to unity, it corresponds to the ratio between two length scales: the typical substrate deformation $\delta \sim 2\eta u^* a(\lambda + 2\mu)/d^*\mu(\lambda + \mu)$ induced by a tangential velocity u^*, and the typical fluid-gap thickness d^*. Throughout the article, we focus on the small-deformation regime of soft-lubrication where $\kappa \ll 1$ (Essink *et al.* 2021).

3. Perturbation theory

We perform a perturbation analysis at small κ (Sekimoto & Leibler 1993; Beaucourt *et al.* 2004; Skotheim & Mahadevan 2004, 2005; Urzay *et al.* 2007; Urzay 2010; Salez & Mahadevan 2015; Pandey *et al.* 2016; Rallabandi *et al.* 2017; Saintyves *et al.* 2020; Zhang *et al.* 2020), as follows:

$$H(R, T) = H_0(R, T) + \kappa H_1(R, T) + O(\kappa^2), \tag{3.1}$$

$$P(R, T) = P_0(R, T) + \kappa P_1(R, T) + O(\kappa^2), \tag{3.2}$$

where the subscript 0 corresponds to the solution for a rigid wall, with $H_0(R, T) = D(T) + R^2$.

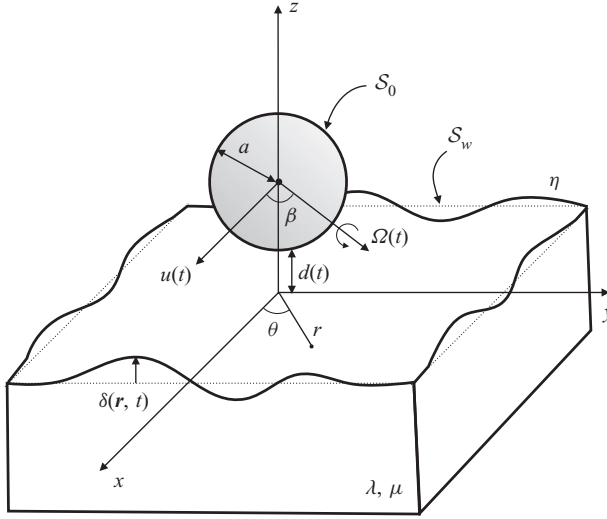Figure 1. Schematic of the system. A rigid sphere of surface $\mathcal{S}_0$ is freely moving in a viscous fluid, near a soft wall of surface $\mathcal{S}_w$ in the flat undeformed state. The lubrication pressure field deforms the latter, which induces an EHD coupling, with forces and torque exerted on the sphere. Note that the surface deformation is magnified for clarity, but that we restrict the analysis to the $\delta \ll d$ case.

3.1. *Zeroth-order solution: rigid wall*

At zeroth order $O(\kappa^0)$, (2.6) reads

$$12\dot{D} = \nabla \cdot \left(H_0^3 \, \nabla P_0 + 6H_0 U \right). \tag{3.3}$$

In polar coordinates, (3.3) can be rewritten as

$$\mathcal{L} \cdot P_0 = R^2 \partial_R^2 P_0 + \left(R + \frac{6R^3}{D + R^2} \right) \partial_R P_0 + \partial_\theta^2 P_0 = \frac{R^2}{(D + R^2)^3} \left(12\dot{D} - 12R \cos\theta \, U \right), \tag{3.4}$$

where $\mathcal{L}$ is a linear operator. We solve this equation using an angular-mode decomposition:

$$P_0(\mathbf{R}, T) = P_0^{(0)}(R, T) + P_0^{(1)}(R, T) \cos\theta, \tag{3.5}$$

where the two coefficients are solutions of the ordinary differential equations

$$R^2 \frac{\mathrm{d}^2 P_0^{(0)}}{\mathrm{d}R^2} + \left(R + \frac{6R^3}{D + R^2} \right) \frac{\mathrm{d}P_0^{(0)}}{\mathrm{d}R} = 12 \frac{R^2 \dot{D}}{(D + R^2)^3}, \tag{3.6a}$$

$$R^2 \frac{\mathrm{d}^2 P_0^{(1)}}{\mathrm{d}R^2} + \left(R + \frac{6R^3}{D + R^2} \right) \frac{\mathrm{d}P_0^{(1)}}{\mathrm{d}R} - P_0^{(1)} = -12 \frac{R^3 U}{(D + R^2)^3}. \tag{3.7a}$$

In accordance with the boundary conditions $P(R \to \infty) = 0$ and $P(R = 0) < \infty$, the solution is thus

$$P_0(\mathbf{R}, T) = -\frac{3\dot{D}}{2(D + R^2)^2} + \frac{6RU \cos\theta}{5(D + R^2)^2}. \tag{3.8}$$
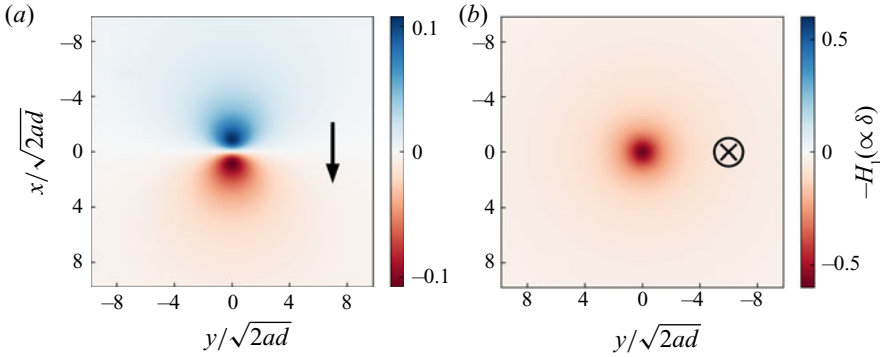
Figure 2. Dimensionless deformation fields at the free surface of the soft substrate, for a sphere placed at a unit distance $D = 1$ and for two modes of motion: (a) the sphere velocity is directed tangentially to the substrate, along the *x*-axis (see black arrow), and is fixed to a unit value $U = 1$; (b) the sphere is approaching the substrate normally (see black cross) with a unit velocity $\dot{D} = -1$.

The first-order substrate deformation H_1 can then be computed from (2.8) at order $O(\kappa)$:

$$H_1(\boldsymbol{R}, T) = \int_{\mathbb{R}^2} \mathrm{d}^2 X \, \frac{P_0(\boldsymbol{X}, T)}{4\pi |\boldsymbol{R} - \boldsymbol{X}|}. \tag{3.9}$$

Using e.g. the spatial Fourier transform $\tilde{H}_1(\boldsymbol{K}) = \int_{\mathbb{R}^2} H_1(\boldsymbol{R}) \exp(-\mathrm{i}\boldsymbol{R} \cdot \boldsymbol{K}) \, \mathrm{d}^2 \boldsymbol{R}$, we find

$$H_1(\boldsymbol{R}, T) = -\frac{3\dot{D}}{8\sqrt{D}} \frac{\mathcal{E}(-R^2/D)}{D + R^2} + \frac{3U}{10R\sqrt{D}} \left(-\frac{D\,\mathcal{E}(-R^2/D)}{D + R^2} + \mathcal{K}(-R^2/D) \right) \cos \theta, \tag{3.10}$$

where $\mathcal{K}$ and $\mathcal{E}$ are the complete elliptic integrals of the first and second kinds (Abramowitz & Stegun 1964). The dimensionless substrate deformations are plotted in figure 2. In figure 2(a), the sphere is moving tangentially to the substrate with a unit velocity $U = 1$. The deformation exhibits a dipolar symmetry, with a negative sign (i.e. the substrate is compressed) at the front. Besides, the isotropic term generated by a sphere moving normally to the substrate is shown in figure 2(b). In particular, for a sphere approaching the substrate, the latter is compressed.

3.2. First-order solution

We can now compute the first-order pressure field P_1 from (2.6) at order $O(\kappa)$:

$$12\partial_T H_1 = \nabla \cdot \left(H_0^3 \nabla P_1 + 3H_0^2 H_1 \nabla P_0 + 6H_1 U \right). \tag{3.11}$$

Invoking the same linear operator $\mathcal{L}$ as in (3.4), we can rewrite (3.11) as

$$\mathcal{L} \cdot P_1 = \frac{R^2}{H_0^3} \left(12\partial_T H_1 - \nabla \cdot \left[3H_0^2 H_1 \nabla P_0 + 6H_1 U \right] \right). \tag{3.12}$$

We then expand all the terms in the right-hand side of (3.12), and we perform once again the angular-mode decomposition:

$$\mathcal{L} \cdot P_1 = F_0(R, T) + F_1(R, T) \cos \theta + F_2(R, T) \cos 2\theta, \tag{3.13}$$

933 A23-6

where we have introduced the auxiliary functions

$$F_0(R, T) = \frac{18R^2 U^2}{25 D^{1/2}(D + R^2)^6} \left[(-10D^2 + 2DR^2)\,\mathcal{E}\left(-\frac{R^2}{D}\right) \right.$$

$$\left. + (8D^2 + 7DR^2 - R^4)\,\mathcal{K}\left(-\frac{R^2}{D}\right) \right]$$

$$+ \frac{9R^2 \dot{D}^2}{4 D^{3/2}(D + R^2)^6} \left[(13D^2 + 3R^2 D + 2R^4)\,\mathcal{E}\left(-\frac{R^2}{D}\right) \right.$$

$$\left. + (-4D^2 - 5R^2 D - R^4)\,\mathcal{K}\left(-\frac{R^2}{D}\right) \right]$$

$$- \frac{9R^2 \ddot{D}\,\mathcal{E}\left(-\dfrac{R^2}{D}\right)}{2 D^{1/2}(D + R^2)^4} \tag{3.14}$$

and

$$F_1(R, T) = -\frac{27 R U \dot{D}}{5 D^{1/2}(D + R^2)^6} \left[(-2D^2 + 7DR^2 + R^4)\,\mathcal{E}\left(-\frac{R^2}{D}\right) \right.$$

$$\left. + 2(D + R^2)(D - R^2)\,\mathcal{K}\left(-\frac{R^2}{D}\right) \right]$$

$$- \frac{18 R \dot{U}}{5 D^{1/2}(D + R^2)^4} \left[-D\,\mathcal{E}\left(-\frac{R^2}{D}\right) + (D + R^2)\,\mathcal{K}\left(-\frac{R^2}{D}\right) \right]. \tag{3.15}$$

Note that we have not provided F_2 as it does not contribute to the forces and torque. Also note that by setting $D(T) = 1$ in the latter expressions, we self-consistently recover the expression of Zhang *et al.* (2020). Invoking the angular-mode decomposition $P_1(R, T) = P_1^{(0)}(R, T) + P_1^{(1)}(R, T)\cos\theta + P_1^{(2)}(R, T)\cos 2\theta$, we get, in particular,

$$R^2 \frac{d^2 P_1^{(0)}}{dR^2} + \left(R + \frac{6R^3}{D + R^2} \right) \frac{dP_1^{(0)}}{dR} = F_0(R, T), \tag{3.16}$$

$$R^2 \frac{d^2 P_1^{(1)}}{dR^2} + \left(R + \frac{6R^3}{D + R^2} \right) \frac{dP_1^{(1)}}{dR} - P_1^{(1)} = F_1(R, T). \tag{3.17}$$

Using scaling arguments, we can write the two relevant first-order pressure components $P_1^{(i)}$ as

$$P_1^{(0)} = \frac{U^2}{D^{7/2}}\,\phi_{U^2}(R/\sqrt{D}) + \frac{\dot{D}^2}{D^{9/2}}\,\phi_{\dot{D}^2}(R/\sqrt{D}) + \frac{\ddot{D}}{D^{7/2}}\,\phi_{\ddot{D}}(R/\sqrt{D}) \tag{3.18}$$

and

$$P_1^{(1)} = \frac{U\dot{D}}{D^4}\,\phi_{U\dot{D}}(R/\sqrt{D}) + \frac{\dot{U}}{D^3}\,\phi_{\dot{U}}(R/\sqrt{D}), \tag{3.19}$$

where the ϕ_i are five dimensionless scaling functions that depend on the self-similar variable $R/\sqrt{D}$ only. Equations (3.18) and (3.19) can be solved numerically with a

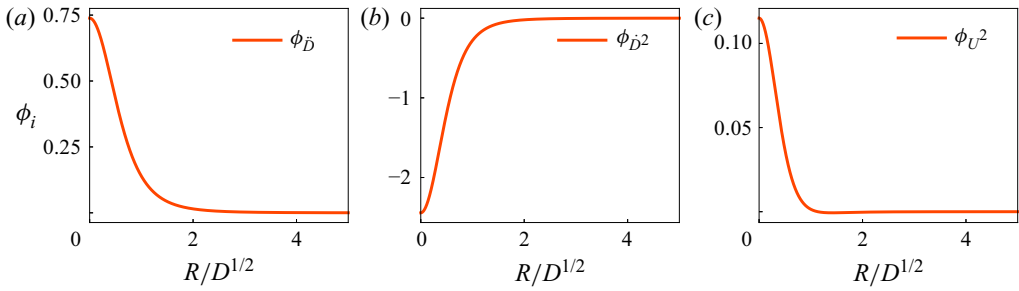*V. Bertin, Y. Amarouchene, E. Raphaël and T. Salez*

Figure 3. Scaling functions for $P_1^{(0)}$ (see (3.18)), obtained from numerical integration of (3.16) with the boundary conditions $\partial_R P_1^{(0)}(R = 0, T) = 0$ and $P_1^{(0)}(R \to \infty, T) = 0$.

Runge–Kutta algorithm and a shooting parameter in order to ensure the boundary condition $P_1(R \to \infty, \theta, T) = 0$. All the scaling functions are plotted in figures 3 and 4.

As a remark, we recall that the substrate deformation is induced by the flow, and that at first order it is linear in the velocity field (see (3.10)). Moreover, the volume-conservation equation involves the time derivative of the fluid-layer thickness, and thus in particular the time derivative of the substrate deformation. As a consequence, when calculating the first-order EHD pressure field, we find terms (and thus forces and torques) that are proportional to the acceleration components $\ddot{D}$ and $\dot{U}$ of the sphere. At first sight, these original inertial-like features might seem inconsistent with steady Stokes flows, but are in fact independent of the fluid density and solely induced by the intimate EHD coupling.

3.3. *Forces and torque*

The force $\boldsymbol{F}$ exerted by the fluid on the sphere is given by

$$\boldsymbol{F} = \int_{\mathcal{S}_0} \boldsymbol{n} \cdot \boldsymbol{\sigma} \, \mathrm{d}s, \tag{3.20}$$

where $\boldsymbol{\sigma} = -p\boldsymbol{I} + \eta(\boldsymbol{\nabla}\boldsymbol{v} + \boldsymbol{\nabla}\boldsymbol{v}^{\mathrm{T}})$ is the fluid stress tensor, $\boldsymbol{n}$ is the unit vector normal to the sphere surface and pointing towards the fluid, and $\boldsymbol{I}$ is the identity tensor. Within the lubrication approximation, the fluid stress tensor reads $\boldsymbol{\sigma} \simeq -p\boldsymbol{I} + \eta\boldsymbol{e}_z\partial_z\boldsymbol{v}$. One can then evaluate the normal force as

$$F_z = \int_{\mathbb{R}^2} p(\boldsymbol{r}) \, \mathrm{d}^2\boldsymbol{r} = -\frac{6\pi\eta a^2 \dot{d}}{d} + 0.41623 \frac{\eta^2 u^2(\lambda + 2\mu)}{\mu(\lambda + \mu)} \left(\frac{a}{d}\right)^{5/2}$$
$$- 41.912 \frac{\eta^2 \dot{d}^2(\lambda + 2\mu)}{\mu(\lambda + \mu)} \left(\frac{a}{d}\right)^{7/2} + 18.499 \frac{\eta^2 \ddot{d}a(\lambda + 2\mu)}{\mu(\lambda + \mu)} \left(\frac{a}{d}\right)^{5/2}, \tag{3.21}$$

where the prefactors have been estimated numerically using (3.18). We recover in particular the classical Reynolds force $-6\pi\eta a^2\dot{d}/d$ at zeroth order, i.e. near a rigid wall. We stress that tangential motions do not induce any normal force at zeroth order in κ, as the corresponding pressure field is antisymmetric in x (see (3.4)). In contrast, such motions do induce a lift force at first order in κ, due to the symmetry breaking of the contact geometry associated with the elastic deformation. Interestingly as well, normal motions generate a viscous adhesive force at first order in compliance (Wang, Feng & Frechette 2020). Besides, an original EHD force proportional to the sphere's normal acceleration is

933 A23-8

also found, as discussed previously. Finally, in Appendix A, and following previous works (Rallabandi *et al.* 2017; Daddi-Moussa-Ider *et al.* 2018; Rallabandi *et al.* 2018; Masoud & Stone 2019), we use the Lorentz reciprocal theorem in order to recover the prefactors of (3.21) analytically, which gives, respectively, $243\pi^3/12800\sqrt{2} \approx 0.41623$, $3915\pi^3/2048\sqrt{2} \approx 41.912$ and $27\pi^3/32\sqrt{2} \approx 18.499$. We note that the latter is in agreement with the result of the linear-response theory derived in Leroy & Charlaix (2011). Furthermore, we recover the lift prefactor (0.416) obtained previously numerically (Zhang *et al.* 2020), as well as analytically in a recently published work (Kargar-Estahbanati & Rallabandi 2021).

Similarly, the tangential force reads

$$F_{\parallel} = \int_{\mathbb{R}^2} \left(-p(\boldsymbol{r}, t) \frac{\boldsymbol{r}}{a} - \eta\partial_z \boldsymbol{v} \right)_{z=h_0(r,t)} \mathrm{d}^2\boldsymbol{r}. \tag{3.22}$$

Using symmetry arguments, we can show that the tangential force is directed along x, i.e. $F_{\parallel} = F_x \boldsymbol{e}_x$. At small κ, we further expand it as $F_x \simeq F_{x,0} + \kappa F_{x,1}$, where $F_{x,0}$ is the viscous drag force applied on a sphere near a rigid plane wall, and $\kappa F_{x,1}$ is the first-order EHD correction. The zeroth-order term cannot be evaluated using the lubrication model introduced in the previous section, because the integral in (3.22) diverges, as the shear term $\eta\partial_z \boldsymbol{v}$ scales as $\sim r^{-2}$ at large r. An exact calculation has been performed using bispherical coordinates and provides a solution in the form of a series expansion (O'Neill 1964). Asymptotic-matching methods have also been employed in order to get the asymptotic behaviour at small d/a (Goldman, Cox & Brenner 1967; O'Neill & Stewartson 1967), which reads $F_{x,0} \approx 6\pi\eta au(\frac{8}{15}\log(d/a) - 0.95429)$ (see Chaoui & Feuillebois (2003) for a high-precision expansion). We note that the sphere's normal velocity does not contribute to the zeroth-order tangential force, as expected by symmetry.

The first-order EHD correction can be computed with the present model, as the correction pressure field and shear stress scale as $\sim r^{-5}$, at large r. It reads

$$F_{x,1} = 2\pi\eta u^* a \int_0^\infty \left[-2RP_1^{(1)} - \frac{H_0}{2}\left(\partial_R P_1^{(1)} + \frac{P_1^{(1)}}{R}\right) \right.$$
$$\left. - \frac{H_1^{(1)}}{2}\partial_R P_0^{(0)} - \frac{H_1^{(0)}}{2}\left(\partial_R P_0^{(1)} + \frac{P_0^{(1)}}{R}\right) + 2\frac{UH_1^{(0)}}{H_0^2} \right] R\,\mathrm{d}R, \tag{3.23}$$

where $H_1^{(i)}$ is the amplitude of the ith mode in the angular-mode decomposition of H_1. Evaluating the latter integral numerically, we find

$$F_x \approx 6\pi\eta au\left(\frac{8}{15}\log\left(\frac{d}{a}\right) - 0.95429\right) - 10.884\frac{\eta^2 u\dot{d}(\lambda+2\mu)}{\mu(\lambda+\mu)}\left(\frac{a}{d}\right)^{5/2}$$
$$+ 0.98661\frac{\eta^2 \dot{u}a(\lambda+2\mu)}{\mu(\lambda+\mu)}\left(\frac{a}{d}\right)^{3/2}. \tag{3.24}$$

We stress that the latter equation is not an exact truncated expansion. In Appendix B, we use again the Lorentz reciprocal theorem in order to compute the first-order EHD force, and we obtain the following analytical expressions for the coefficients of (3.24): $-(3177\pi^3/6400\sqrt{2}) \simeq -10.884$ and $9\pi^3/200\sqrt{2} \simeq 0.98661$, respectively.

The torque exerted by the fluid on the sphere, with respect to its centre of mass, is given by

$$T = \int_{\mathcal{S}_0} a\boldsymbol{n} \times (\boldsymbol{n} \cdot \boldsymbol{\sigma}) \, \mathrm{d}s. \tag{3.25}$$

The latter is directed along the y-direction for symmetry reasons, i.e. $\boldsymbol{T} = T_y \boldsymbol{e}_y$. At small κ, we further expand it as $T_y \simeq T_{y,0} + \kappa T_{y,1}$. For the same reason as with the the viscous drag force near a rigid wall, the viscous torque near a rigid wall cannot be computed within the lubrication model. Using asymptotic-matching methods (O'Neill & Stewartson 1967; Chaoui & Feuillebois 2003), it is found to be $T_{y,0} \approx 8\pi\eta u a^2 (-\frac{1}{10} \log(\frac{d}{a}) - 0.19296)$. In contrast, the first-order EHD correction can be computed with the present model, and reads

$$T_{y,1} = -2\eta u^* a^2 \pi \int_0^\infty \left[\frac{H_0}{2} \left(\partial_R P_1^{(1)} + \frac{P_1^{(1)}}{R} \right) + \frac{H_1^{(1)}}{2} \partial_R P_0^{(0)} \right.$$
$$\left. + \frac{H_1^{(0)}}{2} \left(\partial_R P_0^{(1)} + \frac{P_0^{(1)}}{R} \right) + 2 \frac{U H_1^{(0)}}{H_0^2} \right] R \, \mathrm{d}R. \tag{3.26}$$

Evaluating the latter integral numerically, we find

$$T_y \approx 8\pi\eta u a^2 \left(-\frac{1}{10} \log\left(\frac{d}{a}\right) - 0.19296 \right) + 10.884 \frac{\eta^2 u a \dot{d}(\lambda + 2\mu)}{\mu(\lambda + \mu)} \left(\frac{a}{d}\right)^{5/2}$$
$$- 0.98661 \frac{\eta^2 \dot{u} a^2(\lambda + 2\mu)}{\mu(\lambda + \mu)} \left(\frac{a}{d}\right)^{3/2}. \tag{3.27}$$

The EHD torque in (3.27) is thus the same as the EHD tangential force in (3.24), up to a dimensional prefactor $-a$, as already observed for the EHD interactions of a rigid cylinder near a soft surface (Salez & Mahadevan 2015).

So far, we have focused on the particular case of a semi-infinite elastic material. In Appendices C and D, we apply the same soft-lubrication approach to other elastic models describing thin substrates, which are also widespread in practice. We find similar expressions, but with different numerical prefactors and scalings with the sphere-wall distance.

4. Rotation

We now add the rotation of the sphere, with angular velocity $\boldsymbol{\Omega}(t)$ in the xy-plane (see figure 1), to the previous translational motion. We define β as the angle between $\boldsymbol{\Omega}$ and the x-axis. We stress that $\boldsymbol{\Omega}$ is not necessarily orthogonal (i.e. $\beta = \pi/2$) to the translation velocity. We discard the rotation along the z-axis (e.g. for a spinner), because it does not induce any soft-lubrication coupling. Finally, the system is equivalent to a purely rotating sphere with angular velocity $\boldsymbol{\Omega}(t)$, near a wall translating with a $-\boldsymbol{u}(t)$ velocity. In such a framework, the fluid velocity field at the sphere surface is $\boldsymbol{v} = -\boldsymbol{\Omega} \times a\boldsymbol{n}$, and thus

$v \simeq -\boldsymbol{\Omega} \times a\boldsymbol{e}_z$. All together, the fluid velocity field is modified as

$$\boldsymbol{v}(\boldsymbol{r}, z, t) = \frac{\nabla p(\boldsymbol{r}, t)}{2\eta}(z - h_0(\boldsymbol{r}, t))(z - \delta(\boldsymbol{r}, t)) - \boldsymbol{u}(t)\frac{h_0(\boldsymbol{r}, t) - z}{h_0(\boldsymbol{r}, t) - \delta(\boldsymbol{r}, t)}$$
$$+ a\,\boldsymbol{\Omega}(t) \times \boldsymbol{e}_z\frac{z - \delta(\boldsymbol{r}, t)}{h_0(\boldsymbol{r}, t) - \delta(\boldsymbol{r}, t)}, \tag{4.1}$$

and the Reynolds equation becomes

$$\partial_t h(\boldsymbol{r}, t) = \nabla \cdot \left(\frac{h^3(\boldsymbol{r}, t)}{12\eta}\nabla p(\boldsymbol{r}, t) + \frac{h(\boldsymbol{r}, t)}{2}\left[\underbrace{\boldsymbol{u}(t) - a\,\boldsymbol{\Omega}(t) \times \boldsymbol{e}_z}_{\tilde{\boldsymbol{u}}}\right]\right). \tag{4.2}$$

The problem is thus formally equivalent to the one of a sphere that is purely translating with effective velocity $\tilde{\boldsymbol{u}}(t) = \boldsymbol{u}(t) - a\,\boldsymbol{\Omega}(t) \times \boldsymbol{e}_z$. Therefore, we can directly apply the results from the previous sections, and write all the forces and torque exerted on the sphere, as

$$F_z = -\frac{6\pi\eta a^2\dot{d}}{d} + \frac{243\pi^3}{12800\sqrt{2}}\frac{\eta^2|\boldsymbol{u} - a\boldsymbol{\Omega} \times \boldsymbol{e}_z|^2}{\mu}\left(\frac{a}{d}\right)^{5/2} - \frac{3915\pi^3}{2048\sqrt{2}}\frac{\eta^2\dot{d}^2}{\mu}\left(\frac{a}{d}\right)^{7/2}$$
$$+ \frac{27\pi^3}{32\sqrt{2}}\frac{\eta^2\ddot{d}a}{\mu}\left(\frac{a}{d}\right)^{5/2}, \tag{4.3}$$

$$\boldsymbol{F}_\| = 6\pi\eta a\boldsymbol{u}\left[\frac{8}{15}\log\left(\frac{d}{a}\right) - 0.95429\right] + 6\pi\eta a^2\boldsymbol{e}_z \times \boldsymbol{\Omega}\left[\frac{2}{15}\log\left(\frac{d}{a}\right) + 0.25725\right]$$
$$- \frac{3177\pi^3}{6400\sqrt{2}}\frac{\eta^2(\boldsymbol{u} - a\boldsymbol{\Omega} \times \boldsymbol{e}_z)\dot{d}}{\mu}\left(\frac{a}{d}\right)^{5/2} + \frac{9\pi^3}{200\sqrt{2}}\frac{\eta^2(\dot{\boldsymbol{u}} - a\dot{\boldsymbol{\Omega}} \times \boldsymbol{e}_z)a}{\mu}\left(\frac{a}{d}\right)^{3/2} \tag{4.4}$$

and

$$\boldsymbol{T}_\| = 8\pi\eta a^2\boldsymbol{e}_z \times \boldsymbol{u}\left[-\frac{1}{10}\log\left(\frac{d}{a}\right) - 0.19296\right] + 8\pi\eta a^3\boldsymbol{\Omega}\left[\frac{2}{5}\log\left(\frac{d}{a}\right) - 0.37085\right]$$
$$+ \frac{3177\pi^3}{6400\sqrt{2}}\frac{\eta^2(\boldsymbol{u} - a\boldsymbol{\Omega} \times \boldsymbol{e}_z)a\dot{d}}{\mu}\left(\frac{a}{d}\right)^{5/2} - \frac{9\pi^3}{200\sqrt{2}}\frac{\eta^2(\dot{\boldsymbol{u}} - a\dot{\boldsymbol{\Omega}} \times \boldsymbol{e}_z)a^2}{\mu}\left(\frac{a}{d}\right)^{3/2}, \tag{4.5}$$

where we have invoked the force and torque induced by the rotation of a sphere near a rigid wall (Goldman *et al.* 1967; Urzay 2010) and where the analytical prefactors are computed in Appendices A and B. We stress that the expressions of the EHD forces and torque for a sphere purely translating near thin elastic substrates, as derived in Appendices C and D, can be generalized to further include the sphere's rotation by similarly following the transformation $\boldsymbol{u}(t) \to \boldsymbol{u}(t) - a\,\boldsymbol{\Omega}(t) \times \boldsymbol{e}_z$.

5. Conclusion

We developed a soft-lubrication model in order to compute the EHD interactions exerted on an immersed sphere undergoing both translational and rotational motions near various
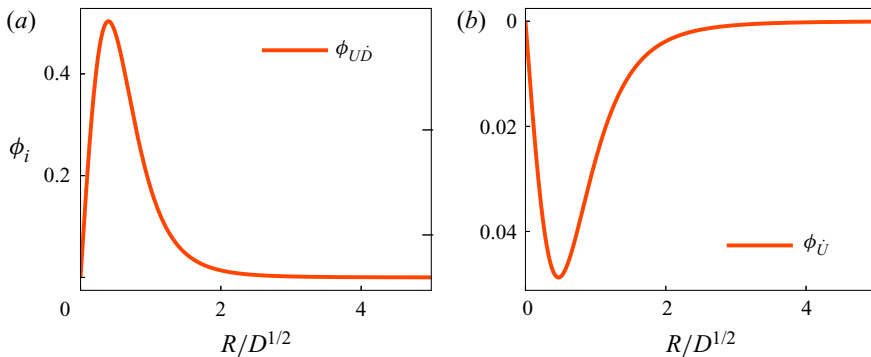
Figure 4. Scaling functions for $P_1^{(1)}$ (see (3.19)), obtained from numerical integration of (3.17), with the boundary conditions $P_1^{(1)}(R = 0, T) = 0$ and $P_1^{(1)}(R \to \infty, T) = 0$.

types of elastic walls. The deformation of the surface was assumed to be small, which allowed us to employ a perturbation analysis in order to obtain the leading-order EHD forces and torque. The obtained interaction matrix exhibits a form that is qualitatively similar to the one found for a two-dimensional cylinder moving near a thin compressible substrate (Salez & Mahadevan 2015). In both cases, the EHD coupling is nonlinear and generates quadratic terms in the sphere velocity, thus breaking the time-reversal symmetry of the Stokes equations. In addition, original inertial-like terms proportional to the acceleration of the sphere are found – despite the assumption of steady flows. Therefore, while the quantitative details such as numerical prefactors and exponents differ in three dimensions and when using more realistic constitutive elastic responses, we expect that the typical zoology of trajectories identified previously (Salez & Mahadevan 2015) will also hold for spherical objects – and will even be extended with the added degree of freedom. As such, the asymptotic predictions obtained here may open new perspectives in colloidal science and biophysics, through the understanding and control of the emerging interactions within soft confinement or assemblies.

Declaration of interests. The authors report no conflict of interest.

Author ORCIDs.
- Vincent Bertin https://orcid.org/0000-0002-3139-8846;
- Yacine Amarouchene https://orcid.org/0000-0002-0475-5510;
- Elie Raphaël https://orcid.org/0000-0003-0007-4790;
- Thomas Salez https://orcid.org/0000-0001-6111-8721.

Appendix A. Lorentz reciprocal theorem: normal force

In this appendix, we compute the first-order normal EHD force using the Lorentz reciprocal theorem for Stokes flows (Rallabandi *et al.* 2017; Daddi-Moussa-Ider *et al.* 2018; Rallabandi *et al.* 2018; Masoud & Stone 2019), in order to recover analytically the numerical prefactors obtained in the main text. To do so, we introduce the model problem of a sphere moving in a viscous fluid and towards an immobile, rigid, planar surface.

We note $\hat{V}_\perp = -\hat{V}_\perp e_z$, the velocity at the particle surface $\mathcal{S}_0$, and we assume a no-slip boundary condition at the undeformed wall surface $\mathcal{S}_w$ located at $z = 0$ (see figure 1). The viscous stress and velocity fields of the model problem follow the steady, incompressible Stokes equations $\nabla \cdot \hat{\sigma}_\perp = \mathbf{0}$ and $\nabla \cdot \hat{v}_\perp = 0$, and we use the lubrication approximation. In this framework, the stress tensor is $\hat{\sigma}_\perp \simeq -\hat{p}_\perp I + \eta e_z \partial_z \hat{v}_\perp$, with

$$\hat{p}_\perp(r) = \frac{3\eta\hat{V}_\perp a}{\hat{h}^2(r)}, \quad \hat{v}_\perp(r, z) = \frac{\nabla\hat{p}_\perp(r)}{2\eta} z(z - \hat{h}(r)), \quad \hat{h}(r) = d + \frac{r^2}{2a}. \quad \text{(A1a–c)}$$

The Lorentz reciprocal theorem states that

$$\int_{\mathcal{S}} \mathbf{n} \cdot \boldsymbol{\sigma} \cdot \hat{v}_\perp \, ds = \int_{\mathcal{S}} \mathbf{n} \cdot \hat{\boldsymbol{\sigma}}_\perp \cdot \mathbf{v} \, ds, \quad \text{(A2)}$$

where $\mathcal{S} = \mathcal{S}_0 + \mathcal{S}_w + \mathcal{S}_\infty$ is the total surface bounding the flow, and $\mathcal{S}_\infty$ is the surface located at $r \to \infty$. The latter does not contribute here. Using the boundary conditions for the model problem, we get

$$\hat{V}_\perp \cdot \mathbf{F} = -\hat{V}_\perp F_z = \int_{\mathcal{S}} \mathbf{n} \cdot \hat{\boldsymbol{\sigma}}_\perp \cdot \mathbf{v} \, ds. \quad \text{(A3)}$$

To find the force exerted on the sphere in the real problem, one needs to specify the boundary conditions for the real velocity field. Here, we assume that the sphere does not rotate, and we describe the flow in the translating reference frame of the particle. The no-slip boundary condition thus reads $\mathbf{v} = \mathbf{0}$ on $\mathcal{S}_0$. We further assume a small deformation of the wall, so that the velocity field at the undeformed wall surface can be obtained using the Taylor expansion:

$$\mathbf{v}|_{z=0} = \mathbf{v}|_{z=\delta} - \delta\partial_z v_0|_{z=0}$$
$$= -u e_x - \dot{d} e_z + (\partial_t - u\partial_x)\delta e_z - \delta\partial_z v_0|_{z=0}, \quad \text{(A4)}$$

where v_0 is the zeroth-order velocity field near a rigid surface. Using results from the main text, we find

$$\partial_z v_0|_{z=0} = -\frac{3\dot{d}r}{\left(d + \dfrac{r^2}{2a}\right)^2} e_r + \frac{2u}{5\left(d + \dfrac{r^2}{2a}\right)} \left(\left(7 - \frac{6d}{d + \dfrac{r^2}{2a}}\right)\cos\theta e_r - \sin\theta e_\theta\right). \quad \text{(A5)}$$

Combining (A1a–c) and (A4), we find the normal force:

$$F_z = \frac{1}{\hat{V}_\perp} \int_{\mathbb{R}^2} \left(\hat{p}_\perp(-\dot{d} + \partial_t\delta - u\partial_x\delta) + \eta\partial_z\hat{v}_\perp|_{z=0} \cdot \partial_z v_0|_{z=0}\delta\right) d\mathbf{r}. \quad \text{(A6)}$$

After some algebra, and computing the integral in Fourier space, we recover the same expression as in (3.21), which reads

$$F_z = -\frac{6\pi\eta a^2\dot{d}}{d} + A\frac{\eta^2 u^2(\lambda + 2\mu)}{\mu(\lambda + \mu)}\left(\frac{a}{d}\right)^{5/2} - B\frac{\eta^2\dot{d}^2(\lambda + 2\mu)}{\mu(\lambda + \mu)}\left(\frac{a}{d}\right)^{7/2}$$
$$+ C\frac{\eta^2\ddot{d}a(\lambda + 2\mu)}{\mu(\lambda + \mu)}\left(\frac{a}{d}\right)^{5/2}, \quad \text{(A7)}$$

where the numerical coefficients A, B, C can be found analytically as

$$A = \frac{9\pi}{25\sqrt{2}} \int_0^\infty k^2 K_0(k) \left(-2K_1(k) + k\, K_2(k)\right) k\, \mathrm{d}k = \frac{243\pi^3}{12\,800\sqrt{2}}, \tag{A8}$$

$$B = 9\pi\sqrt{2} \int_0^\infty k^2 K_1(k) \left(K_2(k) - \frac{k\, K_3(k)}{8}\right) k\, \mathrm{d}k = \frac{3915\pi^3}{2048\sqrt{2}}, \tag{A9}$$

$$C = \frac{9\sqrt{2}\pi}{2} \int_0^\infty k^2 K_1^2(k)\, \mathrm{d}k = \frac{27\pi^3}{32\sqrt{2}}, \tag{A10}$$

and where K_i is the modified Bessel function of the second kind of order i (Abramowitz & Stegun 1964).

Appendix B. Lorentz reciprocal theorem: tangential force

In order to compute the tangential force acting on the particle, we apply the Lorentz reciprocal theorem, but we introduce a different model problem with respect to the previous section. We consider a sphere translating parallel to a rigid immobile substrate, with a velocity $\hat{V}_\parallel$ along the x-axis, and no-slip boundary conditions at both the sphere and substrate surfaces. The velocity and stress fields are denoted $\hat{\sigma}_\parallel$ and $\hat{v}_\parallel$, respectively, and are solutions of the Stokes equations. The lubrication approximation is used here. The solution reads

$$\hat{p}_\parallel(\boldsymbol{r}) = \frac{6\eta \hat{V}_\parallel r \cos\theta}{5\hat{h}^2(\boldsymbol{r})}, \quad \hat{v}_\parallel(\boldsymbol{r}, z) = \frac{\nabla \hat{p}_\parallel(\boldsymbol{r})}{2\eta} z(z - \hat{h}(\boldsymbol{r})) + \hat{V}_\parallel \frac{z}{\hat{h}(\boldsymbol{r})}, \tag{B1a,b}$$

as shown in the main text. The Lorentz reciprocal theorem leads to

$$\hat{V}_\parallel \cdot \boldsymbol{F} = \hat{V}_\parallel F_x = \int_{\mathcal{S}} \boldsymbol{n} \cdot \hat{\boldsymbol{\sigma}}_\parallel \cdot \boldsymbol{v}\, \mathrm{d}s. \tag{B2}$$

Using the lubrication expression of the stress tensor of the model problem, $\hat{\boldsymbol{\sigma}}_\parallel \simeq -\hat{p}_\parallel \boldsymbol{I} + \eta \boldsymbol{e}_z \partial_z \hat{\boldsymbol{v}}_\parallel$, we get an expression for the tangential force as

$$F_x = \frac{1}{\hat{V}_\parallel} \int_{\mathbb{R}^2} \left[-\eta \partial_z \hat{\boldsymbol{v}}_\parallel \cdot u(t)\, \boldsymbol{e}_x - \hat{p}_\parallel (\partial_t - u(t)\, \partial_x)\delta - \eta(\partial_z \hat{\boldsymbol{v}}_\parallel \cdot \partial_z \boldsymbol{v}_0)\delta\right] \mathrm{d}\boldsymbol{r}. \tag{B3}$$

For the same reason as the one invoked in the main text, the zeroth-order tangential drag force (i.e. the integral of $-\eta \partial_z \hat{\boldsymbol{v}}_\parallel \cdot u(t)\boldsymbol{e}_x$ in (B4)) cannot be computed here as the integral diverges within the lubrication approximation. In contrast, the first-order EHD force is well defined in the lubrication framework and can be computed in Fourier space using Parseval's theorem, leading to

$$\kappa F_{x,1} = -\frac{3177\pi^3}{6400\sqrt{2}} \frac{\eta^2 u \dot{d}(\lambda + 2\mu)}{\mu(\lambda + \mu)} \left(\frac{a}{d}\right)^{5/2} + \frac{9\pi^3}{200\sqrt{2}} \frac{\eta^2 \dot{u} a(\lambda + 2\mu)}{\mu(\lambda + \mu)} \left(\frac{a}{d}\right)^{3/2}. \tag{B4}$$

Appendix C. Thin compressible substrate

In this appendix, we derive the EHD interactions exerted on a sphere immersed in a viscous fluid and near a thin compressible substrate of thickness h_{sub}. The deformation field follows the Winkler foundation

$$\delta(\boldsymbol{r}, t) = -\frac{h_{sub}}{(2\mu + \lambda)} p(\boldsymbol{r}, t), \tag{C1}$$

which is valid for substrates of thickness smaller than the typical extent of the pressure field, namely the hydrodynamic radius $\sqrt{2ad}$ (Leroy & Charlaix 2011; Chandler & Vella 2020; Kargar-Estahbanati & Rallabandi 2021). We perform the same asymptotic expansion as the one in the main text, defining the Winkler dimensionless compliance as (Salez & Mahadevan 2015)

$$\kappa^W = \frac{\sqrt{2}h_{sub}\eta u^* a^{1/2}}{d^{*5/2}(2\mu + \lambda)}. \tag{C2}$$

The first-order substrate deformation, or equivalently here the zeroth-order pressure, reads

$$H_1^W(\boldsymbol{R}, T) = P_0(\boldsymbol{R}, T) = \frac{3\dot{D}}{2(D + R^2)^2} + \frac{6RU\cos\theta}{5(D + R^2)^2}. \tag{C3}$$

The first-order deformation fields are plotted in figure 5(*a,b*) for tangential and normal motions of the sphere, respectively. The deformation exhibits the same structure as the one in figure 2 for semi-infinite substrates, but the lateral extent of the deformation is narrower. This is expected as the deformation response induced by a given applied pressure is local for a thin compressible layer (see (C1)), while semi-infinite substrates display a non-local response due to the convolution of the pressure with their Green's function (see (2.3)). The first-order pressure correction follows the same type of equation as in the main text:

$$\mathcal{L} \cdot P_1^W = F_0^W(R, T) + F_1^W(R, T)\cos\theta + F_2^W(R, T)\cos 2\theta, \tag{C4}$$

with

$$\begin{aligned}
F_0^W(R, T) = &-\frac{144R^2 U^2}{25(D + R^2)^7}[D^2 - 6DR^2 + R^4] \\
&+ \frac{18R^2\dot{D}^2}{(D + R^2)^7}[5D - 4R^2] - \frac{18R^2\ddot{D}}{(D + R^2)^5}
\end{aligned} \tag{C5}$$

and

$$F_1^W(R, T) = \frac{216R^3 U\dot{D}}{5(D + R^2)^7}[-5D + R^2] + \frac{72RU}{5(D + R^2)^5}. \tag{C6}$$

We note that F_2^W does not contribute for the forces and torque. The isotropic component of the pressure can be found analytically, using polynomial fractions, as

$$P_1^{W,(0)}(R, T) = \frac{9}{125}\frac{7 - 5Y^2}{(1 + Y^2)^5}\frac{U^2}{D^4} - \frac{3}{40}\frac{71 + 55Y^2 + 30Y^4}{(1 + Y^2)^5}\frac{\dot{D}^2}{D^5} + \frac{3}{2}\frac{1}{(1 + Y^2)^3}\frac{\ddot{D}}{D^4}, \tag{C7}$$

where $Y = R/D^{1/2}$ is the self-similar variable. However, the first angular component of the pressure does not exhibit such an analytical solution, and is thus found by numerical

integration of two scaling functions. Its general expression reads

$$P_1^{W,(1)}(R, T) = \frac{U\dot{D}}{D^{9/2}} \phi_{U\dot{D}}^W \left(\frac{R}{D^{1/2}}\right) + \frac{\dot{U}}{D^{7/2}} \phi_{\dot{U}}^W \left(\frac{R}{D^{1/2}}\right). \tag{C8}$$

Following the same calculation as in the main text, we find the normal force as

$$F_z^W = -\frac{6\pi\eta a^2 \dot{d}}{d} + \frac{48\pi}{125} \frac{\eta^2 u^2 h_{sub}}{a(2\mu + \lambda)} \left(\frac{a}{d}\right)^3 - \frac{72\pi}{5} \frac{\eta^2 \dot{d}^2 h_{sub}}{a(2\mu + \lambda)} \left(\frac{a}{d}\right)^4$$
$$+ \frac{6\pi\eta^2 \ddot{d} h_{sub}}{(2\mu + \lambda)} \left(\frac{a}{d}\right)^3. \tag{C9}$$

We stress that the prefactors $48\pi/125$ and 6π are in agreement with the results in Urzay *et al.* (2007) and Leroy & Charlaix (2011), respectively. Similarly, the force along x reads

$$F_x^W = 6\pi\eta au \left(\frac{8}{15} \log\left(\frac{d}{a}\right) - 0.95429\right) - \frac{484\pi}{125} \frac{\eta^2 u \dot{d} h_{sub}}{a(2\mu + \lambda)} \left(\frac{a}{d}\right)^3$$
$$+ \frac{12\pi}{25} \frac{\eta^2 \dot{u} h_{sub}}{(2\mu + \lambda)} \left(\frac{a}{d}\right)^2, \tag{C10}$$

The torque can be evaluated as well, and reads

$$T_y^W = 8\pi\eta u a^2 \left(-\frac{1}{10} \log\left(\frac{d}{a}\right) - 0.19296\right) + \frac{484\pi}{125} \frac{\eta^2 u \dot{d} h_{sub}}{(2\mu + \lambda)} \left(\frac{a}{d}\right)^3$$
$$- \frac{12\pi}{25} \frac{\eta^2 \dot{u} a h_{sub}}{(2\mu + \lambda)} \left(\frac{a}{d}\right)^2. \tag{C11}$$

All the prefactors for the EHD corrections of the tangential force and torque have been found analytically with the Lorentz reciprocal theorem (see Appendix B). Finally, following the approach in the main text, it is straightforward to generalize (C9), (C10) and (C11) in order to incorporate rotation.

Appendix D. Thin incompressible substrate

In this appendix, we suppose that the substrate of thickness h_{sub} is incompressible, i.e. of Poisson ratio $\nu = 1/2$, which means that the first Lamé coefficient λ is infinite. In this situation, the Winkler foundation is not valid. Instead, the mechanical response of a thin substrate follows the relation (Leroy & Charlaix 2011; Chandler & Vella 2020)

$$\delta(\boldsymbol{r}, t) = \frac{h_{sub}^3}{3\mu} \nabla^2 p(\boldsymbol{r}, t), \tag{D1}$$

where ∇^2 denotes the two-dimensional Laplacian operator in the (x, y)-plane. We perform the same asymptotic expansion as in the main text, defining the thin-incompressible
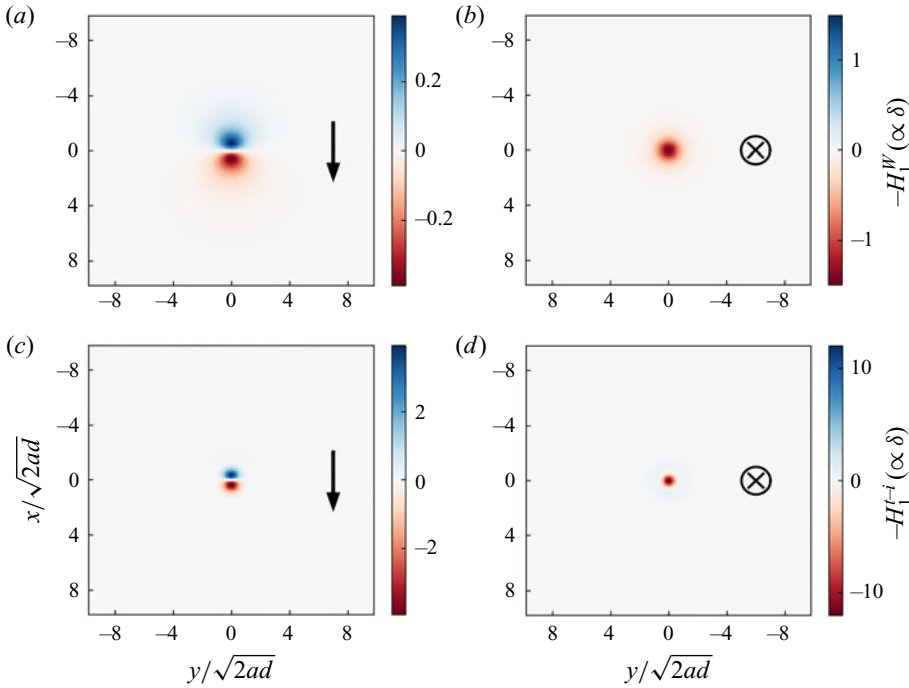
933 A23-16

Figure 5. Dimensionless deformation fields at the free surface of two soft substrates, for a sphere placed at a unit distance $D = 1$ and for two modes of motion. In (a,b), the substrate's mechanical response follows the Winkler foundation (see (C1)). In (c,d), the substrate's mechanical response is the one of a thin incompressible layer (see (D1)).

dimensionless compliance as

$$\kappa^{t-i} = \frac{\eta u^* h_{sub}^3}{3\sqrt{2}\mu d^{*7/2}a^{1/2}}. \tag{D2}$$

The first-order substrate deformation reads

$$H_1^{t-i}(\boldsymbol{R}, T) = -\nabla^2 P_0(\boldsymbol{R}, T) = -\frac{12\dot{D}(D - 2R^2)}{(D + R^2)^4} + \frac{48RU(2D - R^2)\cos\theta}{5(D + R^2)^4}. \tag{D3}$$

The deformation fields are plotted in figure 5(c,d), for tangential and normal motions of the sphere, respectively. The first-order pressure correction follows the same type of equation as in the main text:

$$\mathcal{L} \cdot P_1^{t-i} = F_0^{t-i}(\boldsymbol{R}, T) + F_1^{t-i}(\boldsymbol{R}, T)\cos\theta + F_2^{t-i}(\boldsymbol{R}, T)\cos 2\theta, \tag{D4}$$

with

$$F_0^{t-i}(\boldsymbol{R}, T) = \frac{1152R^2 U^2 (R^2 - 2D)(+2D^2 - 11R^2D + 2R^4)}{25(D + R^2)^9}$$

$$+ \frac{432R^2(2D(D - 5R^2) + 3R^4)\dot{D}^2}{(D + R^2)^9} + \frac{144R^2(2R^2 - D)\ddot{D}}{(D + R^2)^7} \tag{D5}$$

933 A23-17

and

$$F_1^{t-i}(R, T) = -\frac{2592 R^3 \dot{D} U \left(7D^2 - 12R^2 D + R^4\right)}{5 \left(D + R^2\right)^9} - \frac{576 R^3 \dot{U} \left(-2D + R^2\right)}{5 \left(D + R^2\right)^7}. \quad \text{(D6)}$$

We note that F_2^{t-i} does not contribute to the forces and torque. The isotropic component of the pressure can be found analytically, using polynomial fractions, as

$$P_1^{t-i,(0)}(R, T) = \frac{288 \left(7Y^4 - 21Y^2 + 17\right)}{875 \left(1 + Y^2\right)^7} \frac{U^2}{D^5} + \frac{126Y^2 - 198}{7 \left(1 + Y^2\right)^7} \frac{\dot{D}^2}{D^6} + \frac{36}{5 \left(1 + Y^2\right)^5} \frac{\ddot{D}}{D^5}, \quad \text{(D7)}$$

where $Y = R/D^{1/2}$ is the self-similar variable. However, the first angular component of the pressure does not exhibit such an analytical solution, and is thus found by numerical integration of two scaling functions. Its general expression reads

$$P_1^{t-i,(1)}(R, T) = \frac{U\dot{D}}{D^{11/2}} \phi_{U\dot{D}}^{t-i} \left(\frac{R}{D^{1/2}}\right) + \frac{\dot{U}}{D^{9/2}} \phi_{\dot{U}}^{t-i} \left(\frac{R}{D^{1/2}}\right). \quad \text{(D8)}$$

Following the same calculation as in the main text, we find the normal force as

$$F_z^{t-i} = -\frac{6\pi \eta a^2 \dot{d}}{d} + \frac{432\pi}{875} \frac{\eta^2 u^2 h_{sub}^3}{a^3 \mu} \left(\frac{a}{d}\right)^4 - \frac{192\pi}{35} \frac{\eta^2 \dot{d}^2 h_{sub}^3}{a^3 \mu} \left(\frac{a}{d}\right)^5$$
$$+ \frac{12\pi}{5} \frac{\eta^2 \ddot{d} h_{sub}^3}{a^2 \mu} \left(\frac{a}{d}\right)^4. \quad \text{(D9)}$$

We stress that the prefactor $12\pi/5$ is consistent with the linear-response theory in Leroy & Charlaix (2011). Similarly, the force along x reads

$$F_x^{t-i} = 6\pi \eta a u \left(\frac{8}{15} \log\left(\frac{d}{a}\right) - 0.95429\right) - \frac{64\pi}{35} \frac{\eta^2 u \dot{d} h_{sub}^3}{a^3 \mu} \left(\frac{a}{d}\right)^4$$
$$+ \frac{32\pi}{125} \frac{\eta^2 \dot{u} h_{sub}^3}{a^2 \mu} \left(\frac{a}{d}\right)^3. \quad \text{(D10)}$$

The torque can be evaluated as well, and reads

$$T_y^{t-i} = 8\pi \eta u a^2 \left(-\frac{1}{10} \log\left(\frac{d}{a}\right) - 0.19296\right) + \frac{64\pi}{35} \frac{\eta^2 u \dot{d} h_{sub}^3}{a^2 \mu} \left(\frac{a}{d}\right)^4$$
$$- \frac{32\pi}{125} \frac{\eta^2 \dot{u} h_{sub}^3}{a \mu} \left(\frac{a}{d}\right)^3. \quad \text{(D11)}$$

Here again, the prefactors of the transverse force and torque are found using the Lorentz reciprocal theorem, as discussed above in Appendices A, B and C. We stress that the thin-incompressible limit is mathematically valid for strictly incompressible substrates, but that its range of application is limited in practice. Indeed, usual elastomers and gels, which are considered as almost incompressible, have a Poisson ratio close to $\nu \simeq 0.49$, and thus a tiny but finite compressibility. In recent studies (Saintyves *et al.* 2016; Rallabandi *et al.* 2017; Saintyves *et al.* 2020), it has been observed that the mechanical

response of very thin incompressible elastic substrates is better described by the Winkler foundation (i.e. thin and compressible) than the thin-incompressible limit discussed here. This observation has then been established on solid theoretical grounds for the EHD lift (Chandler & Vella 2020), and is intimately rooted in the structure of the elastic Green's function. An empirical scaling, based on the numerical calculation of the EHD lift coefficient, has been derived subsequently (Kargar-Estahbanati & Rallabandi 2021) and suggests that the thin-incompressible model is valid for thicknesses comprised in the range $\frac{\sqrt{7}}{3}(1/2 - \nu)^{1/2} \ll h_{sub}/\sqrt{2ad} \le 0.12$. For $\nu = 0.49$, the lower bound of the latter range is 0.088, which confirms that the validity window of the thin-incompressible model is limited.

REFERENCES

ABKARIAN, M., LARTIGUE, C. & VIALLAT, A. 2002 Tank treading and unbinding of deformable vesicles in shear flow: determination of the lift force. *Phys. Rev. Lett.* **88** (6), 068103.

ABRAMOWITZ, M. & STEGUN, I.A. 1964 *Handbook of Mathematical Functions with Formulas, Graphs, and Mathematical Tables*, vol. 55. US Government Printing Office.

BEAUCOURT, J., BIBEN, T. & MISBAH, C. 2004 Optimal lift force on vesicles near a compressible substrate. *Europhys. Lett.* **67** (4), 676.

BERTIN, V., ZHANG, Z., BOISGARD, R., GRAUBY-HEYWANG, C., RAPHAEL, E., SALEZ, T. & MAALI, A. 2021 Contactless rheology of finite-size air-water interfaces. *Phys. Rev. Res.* **3**, L032007.

BOCQUET, L. & CHARLAIX, E. 2010 Nanofluidics, from bulk to interfaces. *Chem. Soc. Rev.* **39** (3), 1073–1095.

BOUCHET, A.-S., CAZENEUVE, C., BAGHDADLI, N., LUENGO, G.S. & DRUMMOND, C. 2015 Experimental study and modeling of boundary lubricant polyelectrolyte films. *Macromolecules* **48**, 2244.

BRODSKY, E.E. & KANAMORI, H. 2001 Elastohydrodynamic lubrication of faults. *J. Geophys. Res.* **106** (B8), 16357–16374.

CAMPBELL, C.S. 1989 Self-lubrication for long runout landslides. *J. Geol.* **97** (6), 653–665.

CHAN, D.Y.C., KLASEBOER, E. & MANICA, R. 2009 Dynamic deformations and forces in soft matter. *Soft Matt.* **5** (15), 2858–2861.

CHANDLER, T.G.J. & VELLA, D. 2020 Validity of Winkler's mattress model for thin elastomeric layers: beyond Poisson's ratio. *Proc. R. Soc. A* **476** (2242), 20200551.

CHAOUI, M. & FEUILLEBOIS, F. 2003 Creeping flow around a sphere in a shear flow close to a wall. *Q. J. Mech. Appl. Maths* **56** (3), 381–410.

DADDI-MOUSSA-IDER, A., RALLABANDI, B., GEKLE, S. & STONE, H.A. 2018 Reciprocal theorem for the prediction of the normal force induced on a particle translating parallel to an elastic membrane. *Phys. Rev. Fluids* **3** (8), 084101.

DAVIES, H.S., DÉBARRE, D., EL AMRI, N., VERDIER, C., RICHTER, R.P. & BUREAU, L. 2018 Elastohydrodynamic lift at a soft wall. *Phys. Rev. Lett.* **120** (19), 198001.

DAVIS, R.H., SERAYSSOL, J.-M. & HINCH, E.J. 1986 The elastohydrodynamic collision of two spheres. *J. Fluid Mech.* **163**, 479–497.

DOWSON, D. & HIGGINSON, G.R. 2014 *Elasto-Hydrodynamic Lubrication: International Series on Materials Science and Technology*. Elsevier.

ESSINK, M.H., PANDEY, A., KARPITSCHKA, S., VENNER, C.H. & SNOEIJER, J.H. 2021 Regimes of soft lubrication. *J. Fluid Mech.* **915**, A49.

GOLDMAN, A.J., COX, R.G. & BRENNER, H. 1967 Slow viscous motion of a sphere parallel to a plane wall – II. Couette flow. *Chem. Engng Sci.* **22** (4), 653–660.

GONDRET, P., LANCE, M. & PETIT, L. 2002 Bouncing motion of spherical particles in fluids. *Phys. fluids* **14** (2), 643–652.

GONG, J.P. 2006 Friction and lubrication of hydrogels – its richness and complexity. *Soft Matt.* **2** (7), 544–552.

GRANDCHAMP, X., COUPIER, G., SRIVASTAV, A., MINETTI, C. & PODGORSKI, T. 2013 Lift and down-gradient shear-induced diffusion in red blood cell suspensions. *Phys. Rev. Lett.* **110** (10), 108101.

GUAN, D., CHARLAIX, E., QI, R.Z. & TONG, P. 2017 Noncontact viscoelastic imaging of living cells using a long-needle atomic force microscope with dual-frequency modulation. *Phys. Rev. Appl.* **8** (4), 044010.

HAPPEL, J. & BRENNER, H. 2012 *Low Reynolds Number Hydrodynamics: With Special Applications to Particulate Media*, vol. 1. Springer Science & Business Media.

HUI, C.-Y., WU, H., JAGOTA, A. & KHRIPIN, C. 2021 Friction force during lubricated steady sliding of a rigid cylinder on a viscoelastic substrate. *Tribol. Lett.* **69** (2), 1–17.

JAHN, S., SEROR, J. & KLEIN, J. 2016 Lubrication of articular cartilage. *Annu. Rev. Biomed. Engng* **18**, 235–258.

JONES, M.B., FULFORD, G.R., PLEASE, C.P., MCELWAIN, D.L.S. & COLLINS, M.J. 2008 Elastohydrodynamics of the eyelid wiper. *Bull. Math. Biol.* **70** (2), 323–343.

KARAN, P., CHAKRABORTY, J. & CHAKRABORTY, S. 2018 Small-scale flow with deformable boundaries. *J. Ind. Inst. Sci.* **98** (2), 159–183.

KARGAR-ESTAHBANATI, A. & RALLABANDI, B. 2021 Lift forces on three-dimensional elastic and viscoelastic lubricated contacts. *Phys. Rev. Fluids* **6** (3), 034003.

LAINÉ, A., JUBIN, L., CANALE, L., BOCQUET, L., SIRIA, A., DONALDSON, S.H. & NIGUÈS, A. 2019 Micromegascope based dynamic surface force apparatus. *Nanotechnology* **30** (19), 195502.

LEROY, S. & CHARLAIX, E. 2011 Hydrodynamic interactions for the measurement of thin film elastic properties. *J. Fluid Mech.* **674**, 389–407.

LEROY, S., STEINBERGER, A., COTTIN-BIZONNE, C., RESTAGNO, F., LÉGER, L. & CHARLAIX, É. 2012 Hydrodynamic interaction between a spherical particle and an elastic surface: a gentle probe for soft thin films. *Phys. Rev. Lett.* **108** (26), 264501.

MASOUD, H. & STONE, H.A. 2019 The reciprocal theorem in fluid dynamics and transport phenomena. *J. Fluid Mech.* **879**, P1.

MEEKER, S.P., BONNECAZE, R.T. & CLOITRE, M. 2004 Slip and flow in soft particle pastes. *Phys. Rev. Lett.* **92** (19), 198302.

MOW, V.C., HOLMES, M.H. & LAI, W.M. 1984 Fluid transport and mechanical properties of articular cartilage: a review. *J. Biomech.* **17** (5), 377–394.

MOYLE, N., WU, H., KHRIPIN, C., BREMOND, F., HUI, C.-Y. & JAGOTA, A. 2020 Enhancement of elastohydrodynamic friction by elastic hysteresis in a periodic structure. *Soft Matt.* **16** (6), 1627–1635.

O'NEILL, M.E. 1964 A slow motion of viscous liquid caused by a slowly moving solid sphere. *Mathematika* **11** (1), 67–74.

O'NEILL, M.E. & STEWARTSON, K. 1967 On the slow motion of a sphere parallel to a nearby plane wall. *J. Fluid Mech.* **27** (4), 705–724.

PANDEY, A., KARPITSCHKA, S., VENNER, C.H. & SNOEIJER, J.H. 2016 Lubrication of soft viscoelastic solids. *J. Fluid Mech.* **799**, 433–447.

RALLABANDI, B., OPPENHEIMER, N., ZION, M.Y.B. & STONE, H.A. 2018 Membrane-induced hydroelastic migration of a particle surfing its own wave. *Nat. Phys.* **14** (12), 1211–1215.

RALLABANDI, B., SAINTYVES, B., JULES, T., SALEZ, T., SCHÖNECKER, C., MAHADEVAN, L. & STONE, H.A. 2017 Rotation of an immersed cylinder sliding near a thin elastic coating. *Phys. Rev. Fluids* **2** (7), 074102.

SAINTYVES, B., JULES, T., SALEZ, T. & MAHADEVAN, L. 2016 Self-sustained lift and low friction via soft lubrication. *Proc. Natl Acad. Sci.* **113** (21), 5847–5849.

SAINTYVES, B., RALLABANDI, B., JULES, T., AULT, J., SALEZ, T., SCHÖNECKER, C., STONE, H.A. & MAHADEVAN, L. 2020 Rotation of a submerged finite cylinder moving down a soft incline. *Soft Matt.* **16**, 4000.

SALEZ, T. & MAHADEVAN, L. 2015 Elastohydrodynamics of a sliding, spinning and sedimenting cylinder near a soft wall. *J. Fluid Mech.* **779**, 181–196.

SEKIMOTO, K. & LEIBLER, L. 1993 A mechanism for shear thickening of polymer-bearing surfaces: elasto-hydrodynamic coupling. *Europhys. Lett.* **23** (2), 113.

SKOTHEIM, J.M. & MAHADEVAN, L. 2004 Soft lubrication. *Phys. Rev. Lett.* **92** (24), 245509.

SKOTHEIM, J.M. & MAHADEVAN, L. 2005 Soft lubrication: the elastohydrodynamics of nonconforming and conforming contacts. *Phys. Fluids* **17** (9), 092101.

SNOEIJER, J.H., EGGERS, J. & VENNER, C.H. 2013 Similarity theory of lubricated hertzian contacts. *Phys. Fluids* **25** (10), 101705.

TAN, M.R., WANG, Y. & FRECHETTE, J. 2019 Criterion for particle rebound during wet collisions on elastic coatings. *Phys. Rev. Fluids* **4** (8), 084305.

URZAY, J. 2010 Asymptotic theory of the elastohydrodynamic adhesion and gliding motion of a solid particle over soft and sticky substrates at low Reynolds numbers. *J. Fluid Mech.* **653**, 391–429.

URZAY, J., LLEWELLYN SMITH, S.G. & GLOVER, B.J. 2007 The elastohydrodynamic force on a sphere near a soft wall. *Phys. Fluids* **19** (10), 103106.

VAKARELSKI, I.U., MANICA, R., TANG, X., O'SHEA, S.J., STEVENS, G.W., GRIESER, F., DAGASTINE, R.R. & CHAN, D.Y.C. 2010 Dynamic interactions between microbubbles in water. *Proc. Natl Acad. Sci.* **107** (25), 11177–11182.

VIALAR, P., MERZEAU, P., GIASSON, S. & DRUMMOND, C. 2019 Compliant surfaces under shear: elastohydrodynamic lift force. *Langmuir* **35** (48), 15605–15613.

VILLEY, R., MARTINOT, E., COTTIN-BIZONNE, C., PHANER-GOUTORBE, M., LÉGER, L., RESTAGNO, F. & CHARLAIX, E. 2013 Effect of surface elasticity on the rheology of nanometric liquids. *Phys. Rev. Lett.* **111** (21), 215701.

VINOGRADOVA, O.I. & FEUILLEBOIS, F. 2000 Elastohydrodynamic collision of two spheres allowing slip on their surfaces. *J. Colloid Interface Sci.* **221** (1), 1–12.

WANG, Y., DHONG, C. & FRECHETTE, J. 2015 Out-of-contact elastohydrodynamic deformation due to lubrication forces. *Phys. Rev. Lett.* **115** (24), 248302.

WANG, Y., FENG, Z. & FRECHETTE, J. 2020 Dynamic adhesion due to fluid infusion. *Curr. Opin. Colloid Interface Sci.* **50**, 101397.

WANG, Y., PILKINGTON, G.A., DHONG, C. & FRECHETTE, J. 2017*a* Elastic deformation during dynamic force measurements in viscous fluids. *Curr. Opin. Colloid Interface Sci.* **27**, 43–49.

WANG, Y., TAN, M.R. & FRECHETTE, J. 2017*b* Elastic deformation of soft coatings due to lubrication forces. *Soft Matt.* **13** (38), 6718–6729.

WANG, Y., ZENG, B., ALEM, H.T., ZHANG, Z., CHARLAIX, E. & MAALI, A. 2018 Viscocapillary response of gas bubbles probed by thermal noise atomic force measurement. *Langmuir* **34** (4), 1371–1375.

WU, H., MOYLE, N., JAGOTA, A. & HUI, C.-Y. 2020 Lubricated steady sliding of a rigid sphere on a soft elastic substrate: hydrodynamic friction in the Hertz limit. *Soft Matt.* **16** (11), 2760–2773.

ZHANG, Z., BERTIN, V., ARSHAD, M., RAPHAEL, E., SALEZ, T. & MAALI, A. 2020 Direct measurement of the elastohydrodynamic lift force at the nanoscale. *Phys. Rev. Lett.* **124** (5), 054502.